KSCE Journal of Civil Engineering
Vol. 6, No. 1 / March 2002
pp. 47~60

Seismic Protection of Nonlinear Coupled Bridge Systems Using Semi-active Control Strategy

By Hyung-Jo Jung*, Anat Ruangrassamee, Kazuhiko Kawashima***, Billie F. Spencer, Jr**** and In-Won Lee*****

Abstract

Under strong ground excitation, a bridge may experience inelastic deformation induced by hysteretic behavior at a plastic hinge of a pier and pounding between the two decks. In this study, the semi-active control strategy using the clipped optimal control algorithm is extended to control a nonlinear coupled bridge system. The nonlinearity caused by plastic deformation of piers is considered in analysis, and the effectiveness of the clipped optimal control is presented.

Key words: clipped optimal control, nonlinear bridge system, pounding, smart dampers, semi-active control

1. Introduction

Under strong ground excitation, pounding may occur between the two decks or between a deck and an abutment in a bridge system. Pounding can result in an increase in the deck response that may, in turn, lead to unseating of decks. In addition, bridges may experience nonlinearity induced by hysteretic behavior at plastic hinges of the piers. Conventionally, the seismic performance of a bridge is assured for some particular target ground motions. Since input ground motion is unpredictable, there arises the need to make structural properties more adaptive to responses. Many researchers have attempted to apply active and semi-active control systems in the civil engineering structures. Active control systems have been proved to reduce structural response. However, the response reduction is obtained at the expense of requiring substantial power. Alternatively, semi-active control systems offer the reliability of passive control systems; yet provide the adaptability of active control systems. Because semi-active control systems are inherently stable and require much less power, application of semi-active control systems to civil engineering structures is very promising. Recently, magneto-rheological (MR) fluid dampers have been developed (Spencer *et al*. 1997; Sunakoda *et al*. 2000). MR fluid dampers can be controlled with small power supplies and the dynamic range of the damping force is quite large. Consequently, full-scale implementation of semi-active control becomes a possible solution.

Many researchers have investigated control algorithms for semi-active control. The performance of the clipped optimal control algorithm was shown to be effective through analytical simulation and small-scale shaking table test (Dyke *et al*. 1996; Johnson *et al*. 1998). It was found that the clipped optimal control algorithm provided response reduction close to that obtained from the active control by linear optimal control. Since the semiactive control force is always dissipative, system stability is assured. Moreover such a damping force generally can be realized using a relatively small power supply. The clipped optimal control and linear optimal control have been developed for linear structures. As mentioned above, nonlinearity is unavoidable when a bridge is subjected to a strong ground motion. This study investigates the effectiveness of the semiactive control of a bridge structure exhibiting inelastic deformation of the piers employing the clipped optimal

*Member, Research Assistant Professor, Dept. of Civil Engrg., KAIST (E-mail: hjung@mail.kaist.ac.kr)
**Graduate Student, Dept. of Civil Engrg., Tokyo Inst. of Tech., Japan (E-mail: anat@cv.titech.ac.jp)
***Professor, Dept. of Civil Engrg., Tokyo Inst. of Tech., Japan (E-mail: kawasima@cv.titech.ac.jp)
****Linbeck Professor, Dept. of Civil Engrg. & Geo. Sci., Univ. of Notre Dame, USA (E-mail: spencer@nd.edu)
*****Member, Professor, Dept. of Civil Engrg., KAIST (E-mail: iwlee@kaist.ac.kr)

The manuscript for this paper was submitted for review on November 9, 2001.

control algorithm.

2. Analytical Model and Equations of Motion

Fig. 1 illustrates a highway bridge consisting of two 5-span continuous decks, which will be considered in this analysis. The reinforce-concrete pier is 10 m high. The decks are of steel I-girders. Each deck is 40 m long and 12 m wide. The total weight of a deck is 31.4 MN. The deck is supported by five 96mm-thick elastomeric bearings on each pier. The size of the elastomeric bearings is 700 mm× 700 mm for the left deck, while it is 990 mm×990 mm for the right deck. Thus, the stiffness of the elastomeric bearings for the right deck is twice that for the left deck.

Based on an eigenvalue analysis of the target bridge using a two-dimensional discrete model, it is found that the natural period of the system of the left deck and supporting piers is 1.13 s and that of the right deck and supporting piers is 0.88 s. The bridge was simplified as two single-degree-of-freedom systems shown in Fig. 2. The systems are referred to as System 1 and System 2, respectively. The restoring spring of System 1 has a yielding stiffness k_{y1}=103.0 MN/m and a yielding displacement u_{y1}=0.241 m. The restoring spring of System 2 has a yielding stiffness k_{y2}=179.8 MN/m and a yielding displacement u_{y2}=0.138 m.

The ductility factor of the deck-bearing-pier system can be estimated from

$$\mu_{si} = \frac{m_i^{max}}{u_y^i} \tag{1}$$

where μ_{si} is the system ductility factor of System i, and u_i^{max} is the maximum displacement of System i. The system ductility capacity of System 1 is equal to 1.93, while that of System 2 is 2.62. Note that the ductility capacity of the pier is equal to 7.4. In addition to the hysteretic damping, damping ratios h_1=h_2=0.05 were assumed for both systems. The mass of System 1, m_1 =3300 ton, and that of System 2, m_2 =3527 ton.

A semi-active control device is provided between Systems 1 and 2. The semi-active control device is intended to reduce the displacement of each system and to reduce the relative displacement between the two systems.

Systems 1 and 2 are subjected to the same ground motion, neglecting spatial variation of a ground motion along the longitudinal direction of the bridge. The ground motion records used in the analysis were:

1) *JMA Kobe record* - The NS component of the ground motion recorded at the JMA Kobe Observatory in the 1995 Hyogo-ken Nanbu earthquake. The earthquake had a magnitude of 7.2 and a focal depth of 14 km. The peak ground acceleration of the record was 8.18 m/s^2.

2) *Sylmar record* - The NS component of the ground motion recorded at a parking lot of the Sylmar County hospital in the 1994 Northridge earthquake. The earthquake had a magnitude of 6.8 and a focal depth of 18 km. The peak ground acceleration for the record is 8.27 m/s^2.

Fig. 3 shows the ground acceleration of these earthquake records.

Denoting the displacement response of two systems relative to the ground by $\boldsymbol{u}(t) = [u_1(t)u_2(t)]^T$, the equations of motion of the bridge system may be presented as

$$\boldsymbol{M}\ddot{\boldsymbol{u}}(t) + \boldsymbol{C}\dot{\boldsymbol{u}}(t) + \boldsymbol{F}_s(\boldsymbol{u}, \dot{\boldsymbol{u}}, t) = \boldsymbol{\Lambda} f(t) - \boldsymbol{M}\mathbf{1}\ddot{u}_g(t) \tag{2}$$

where $M=\begin{bmatrix} m_1 & 0 \\ 0 & m_2 \end{bmatrix}$, $C=\begin{bmatrix} 2h_1\sqrt{k_{y1}\cdot m_2} & 0 \\ 0 & 2h_2\sqrt{k_{y2}\cdot m_2} \end{bmatrix}$, $L=[-1\ 1]^T$, indicating the location of the control device, $f(t)$ is the control force, **1** is a column vector of ones, $\ddot{u}_g(t)$ is the ground acceleration, and $\boldsymbol{F}_s(\boldsymbol{u}, \dot{\boldsymbol{u}}, t)$ is the matrix of restoring forces. Note that the control force is defined as positive for the compressive

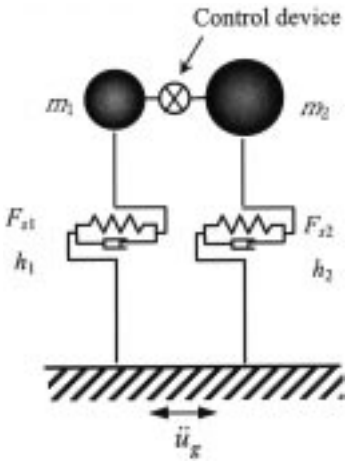

Fig. 2. Analytical Model

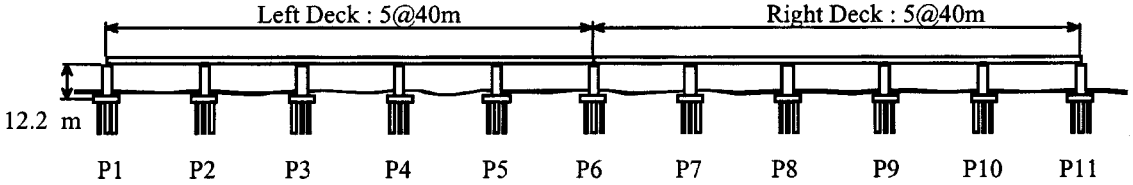

Fig. 1. Target Bridge

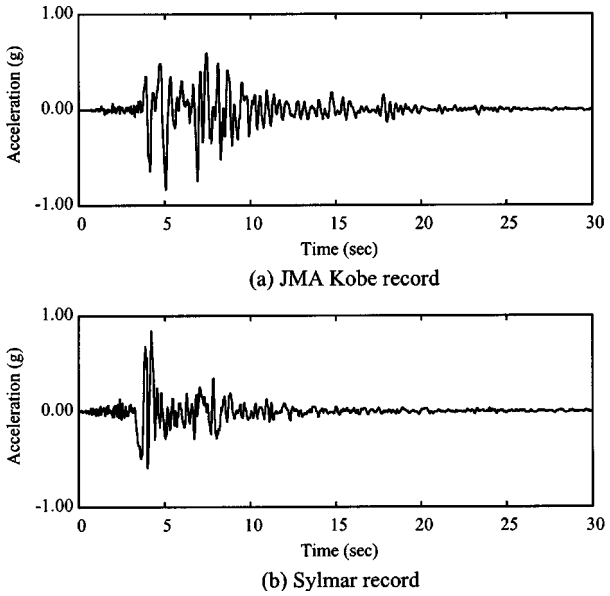

Fig. 3. Ground Acceleration of the Ground Motion Records Used in Analysis

force in the control device. The matrix of nonlinear restoring forces $\boldsymbol{F}_s(\boldsymbol{u}, \dot{\boldsymbol{u}}, t)$ is expressed as

$$\boldsymbol{F}_s(\boldsymbol{u}, \dot{\boldsymbol{u}}, t) = \begin{bmatrix} F_{s1}(\boldsymbol{u}, \dot{\boldsymbol{u}}, t) & 0 \\ 0 & F_{s2}(\boldsymbol{u}, \boldsymbol{u}, t) \end{bmatrix} \tag{3}$$

The restoring force $\boldsymbol{F}_{s1}(\boldsymbol{u}, \dot{\boldsymbol{u}}, t)$ and $\boldsymbol{F}_{s2}(\boldsymbol{u}, \dot{\boldsymbol{u}}, t)$ are decomposed as

$$F_{si}(\boldsymbol{u}, \dot{\boldsymbol{u}}, t) = \alpha_i k_{yi} u_i(t) + (1-\alpha_i) k_{yi} u_{yi} v_i(t); \quad i = 1, 2 \tag{4}$$

where α_i is the stiffness ratio of the post-yielding stiffness to the yielding stiffness and $v_i(t)$ is the variable representing the hysteresis behavior by the Bouc-Wen model (Wen 1976). The Bouc-Wen model is expressed in the form of a differential equation as

$$\dot{v}_i = \frac{\gamma |\dot{u}_i(t)||v_i(t)|^{n-1} v_i(t) - \beta \dot{u}_i(t) |v_i(t)|^n + A\dot{u}_i(t)}{u_{yi}(t)}$$
$$i = 1, 2 \tag{5}$$

in which the parameters γ, β, and A govern the shape of a hysteresis loop, and the parameter n governs the smoothness of the transition from the pre-yielding to the post-yielding region. It is important to note that degradation of stiffness in terms of displacement cannot be represented by this Bouc-Wen model. Substituting Equation (4) into Equation (3), can be rewritten as follows:

$$\boldsymbol{F}_s(t) = \boldsymbol{K}_L \boldsymbol{u}(t) + \boldsymbol{K}_{NL} \boldsymbol{v}(t) \tag{6}$$

where $\boldsymbol{K}_L$ is a diagonal matrix with elements $\alpha_i k_{yi}$ (i=1, 2), and is a diagonal matrix with elements (i=1, 2). Substituting Equation (6) into Equation (2) leads to

$$\boldsymbol{M}\ddot{\boldsymbol{u}}(t) + \boldsymbol{C}\dot{\boldsymbol{u}}(t) + \boldsymbol{K}_L \boldsymbol{u}(t) = \Lambda f(t) - \boldsymbol{M}\boldsymbol{1} u_g(t) - \boldsymbol{K}_{NL} v(t) \tag{7}$$

In the state-space representation, Equation (7) can be expressed as

$$\dot{\boldsymbol{z}}(t) = \boldsymbol{A}\boldsymbol{z}(t) + \boldsymbol{B}f(t) + \boldsymbol{E}\ddot{\boldsymbol{u}}_g(t) + \boldsymbol{H}\boldsymbol{v}(t) \tag{8}$$

where

$$\boldsymbol{z}(t) = [\boldsymbol{u}(t) \;\; \dot{\boldsymbol{u}}(t)]^T, \boldsymbol{A} = \begin{bmatrix} \boldsymbol{0} & \boldsymbol{I} \\ -\boldsymbol{M}^{-1}\boldsymbol{K}_L & -\boldsymbol{M}^{-1}\boldsymbol{C} \end{bmatrix},$$
$$\boldsymbol{B} = \begin{bmatrix} \boldsymbol{0} \\ \boldsymbol{M}^{-1}\boldsymbol{\Lambda} \end{bmatrix}, \boldsymbol{E} = \begin{bmatrix} \boldsymbol{0} \\ -\boldsymbol{1} \end{bmatrix}, \boldsymbol{H} = \begin{bmatrix} \boldsymbol{0} \\ \boldsymbol{M}^{-1}\boldsymbol{K}_{NL} \end{bmatrix}$$

3. Semi-active Control Strategy Using Clipped Optimal Control Algorithm

Fig. 4 shows the conceptual block diagram of the semi-active control strategy using the clipped optimal control algorithm. The structure represented by the state-space form in Equation (8) is subjected to a ground excitation. The displacement and velocity responses are the output from the structure. Based on the measured state, the desired control force is commanded. The control force is determined from

$$f(t) = -K_c z(t) \tag{9}$$

which is the multiplication of the measured full-state with the constant gain matrix $\boldsymbol{K}_c$. In this study, the linear quadratic regulator (LQR) optimal control was employed to design the controller.

Note that in the design of the controller, the structure is assumed linear (α_i in Equation (4) is equal to 1). For control design, the following cost function was minimized.

$$J = \left[\int_0^t (y^T Q y + r f^2) dt \right] \tag{10}$$

where $\boldsymbol{Q}$ is the weighting matrix of output response **y**, and r is the weighting parameter for the control effort. The weight value r was set equal to 1.0. The weighting matrix $\boldsymbol{Q}$ can be written as

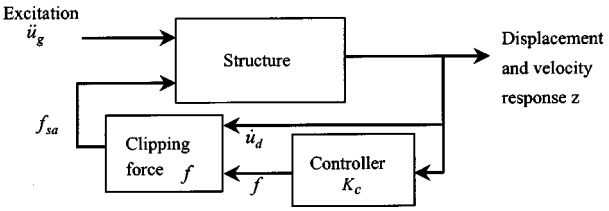

Fig. 4. Block Diagram of the Semi-Active Control Strategy Using the Clipped Optimal Control Algorithm

$$\boldsymbol{Q} = \begin{bmatrix} q_{dis} & 0 & 0 & 0 & 0 & 0 & 0 & 0 \\ 0 & q_{dis} & 0 & 0 & 0 & 0 & 0 & 0 \\ 0 & 0 & q_{vel} & 0 & 0 & 0 & 0 & 0 \\ 0 & 0 & 0 & q_{vel} & 0 & 0 & 0 & 0 \\ 0 & 0 & 0 & 0 & q_{acc} & 0 & 0 & 0 \\ 0 & 0 & 0 & 0 & 0 & q_{acc} & 0 & 0 \\ 0 & 0 & 0 & 0 & 0 & 0 & q_{reldis} & 0 \\ 0 & 0 & 0 & 0 & 0 & 0 & 0 & q_{relvel} \end{bmatrix} \tag{11}$$

where q_{dis} is the weighting parameter for the displacement of each system, q_{vel} is the weighting value of velocity of each system, q_{acc} is the weighting parameter for the acceleration of each system, $q_{rel\ dis}$ is the weighting parameter for the relative displacement between the two systems, and $q_{rel\ vel}$ is the weighting parameter for the relative velocity between two systems. Since ground motions are random in nature, containing a wide range of frequency components, the controller design was conducted assuming that the input is a white noise process. The root-mean-square (RMS) value is used to characterize the response of the structure. Based on a series of analyses, the weighing values were chosen as 10^{16} for the displacement and 10^{15} for the relative displacement between the two systems. For these weighting values, the control gain matrix $\boldsymbol{K_c}$ was obtained as

$$K_c = [-2.471 \quad 6.056 \quad -1.525 \quad 0.655] \times 10^7 \quad (Unit\ in\ N,m,s) \tag{12}$$

Similar to a passive control device, the damping force of a semi-active damper has the same sign as the velocity of the damper. Therefore, a secondary bang-bang controller functions to clip the forces that cannot be realized by a semi-active damper. The secondary controller can be expressed as

$$f_{sa} = \begin{cases} f & f \cdot \dot{u}_d > 0 \\ 0 & f \cdot \dot{u}_d \le 0 \end{cases} \tag{13}$$

where f_{sa} is the control force to the semi-active, f is the control force commanded by the linear optimal controller, and $\dot{u}_d$ is the velocity of the damper. Note that the control force and the displacement of the damper are defined as positive for the compression.

4. Effectiveness of Clipped Optimal Control Algorithm

Fig. 5 shows the response of the bridge subjected to the JMA Kobe record when no control device is provided. The maximum displacements of Systems 1 and 2 are 0.29 m and 0.24 m, respectively. The relative displacement between the two systems is 0.29 m. From the restoring force

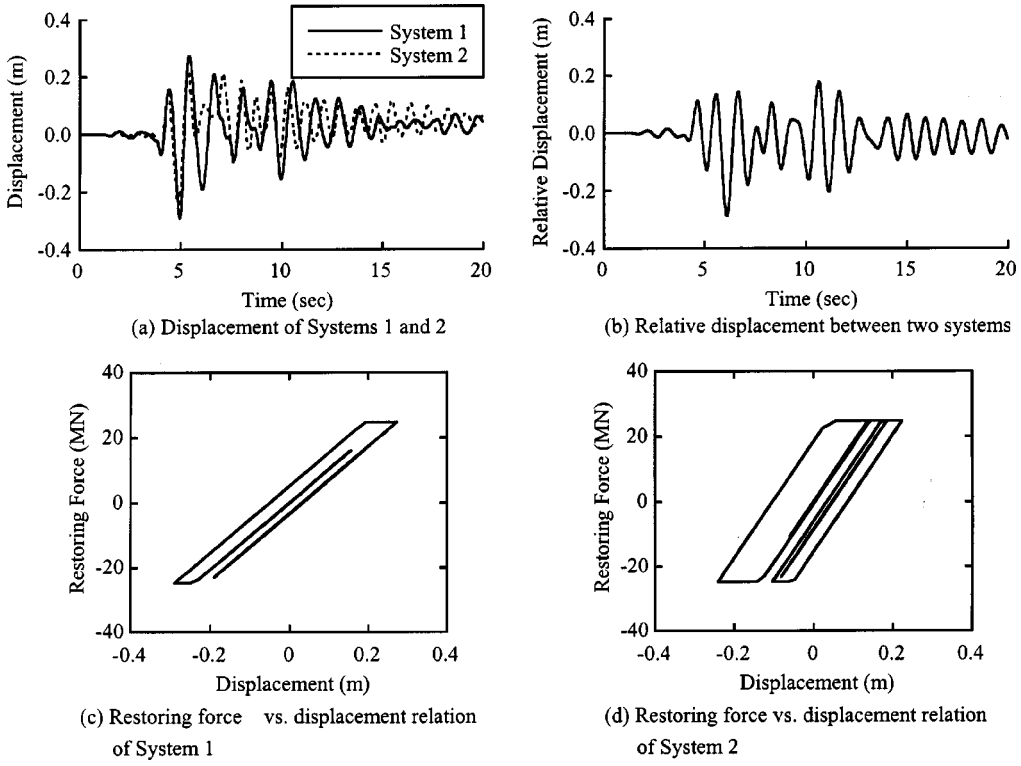

(a) Displacement of Systems 1 and 2

(b) Relative displacement between two systems

(c) Restoring force vs. displacement relation of System 1

(d) Restoring force vs. displacement relation of System 2

Fig. 5. Response of the Bridge Without Control (JMA Kobe record)

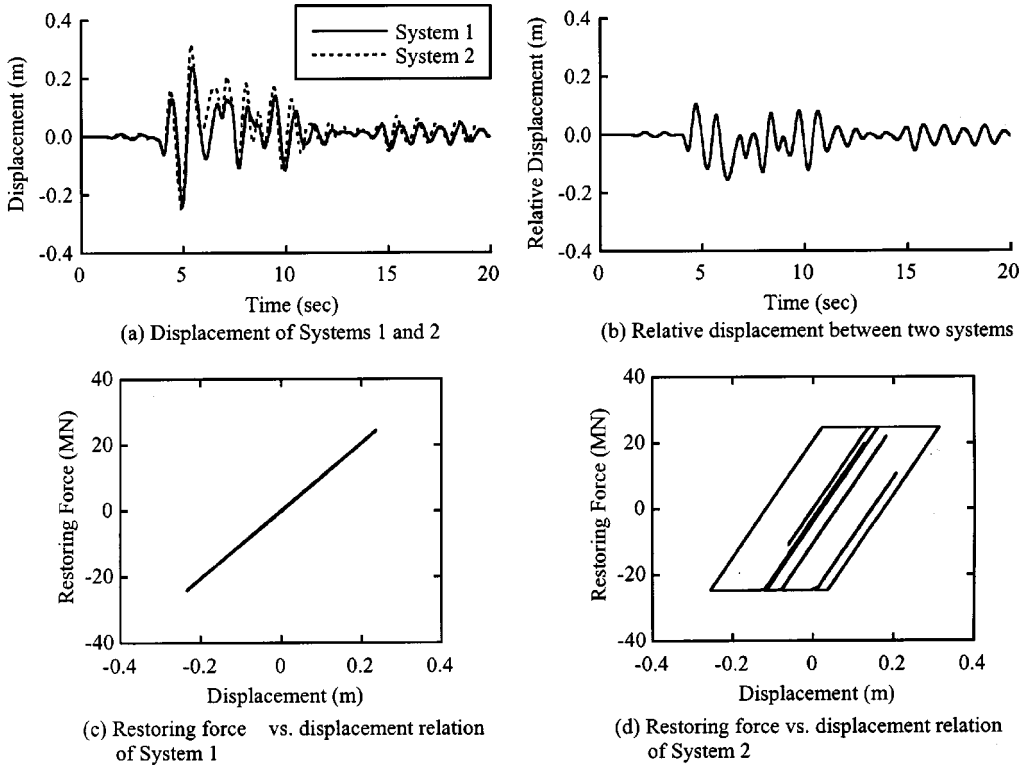

Fig. 6. Response of the Bridge with Active Control (JMA Kobe Record)

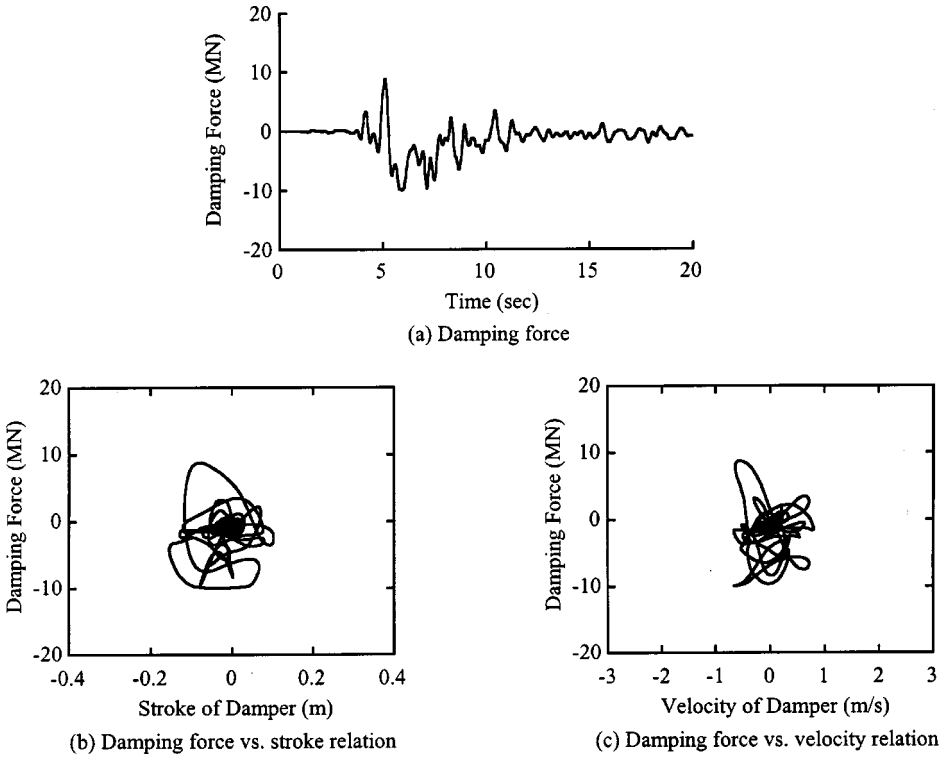

Fig. 7. Response of the Control Device with Active Control (JMA Kobe record)

vs. displacement relation, it is seen that System 2 experiences more nonlinearity than System 1. The response ductility factor is 1.21 for System 1 and 1.75 for System 2.

Since the clipped optimal control algorithm inherits a major part from the linear optimal control algorithm, it is worthy to proceed from the linear optimal control (which will be referred to as the active control hereafter). Fig. 6 shows the response of the bridge when active control is applied. The relative displacement between the two systems is 0.16 m. The displacement of System 1 decreases to 0.24 m, while that of System 2 increases to 0.31 m. Thus, the response ductility factor of System 1 becomes

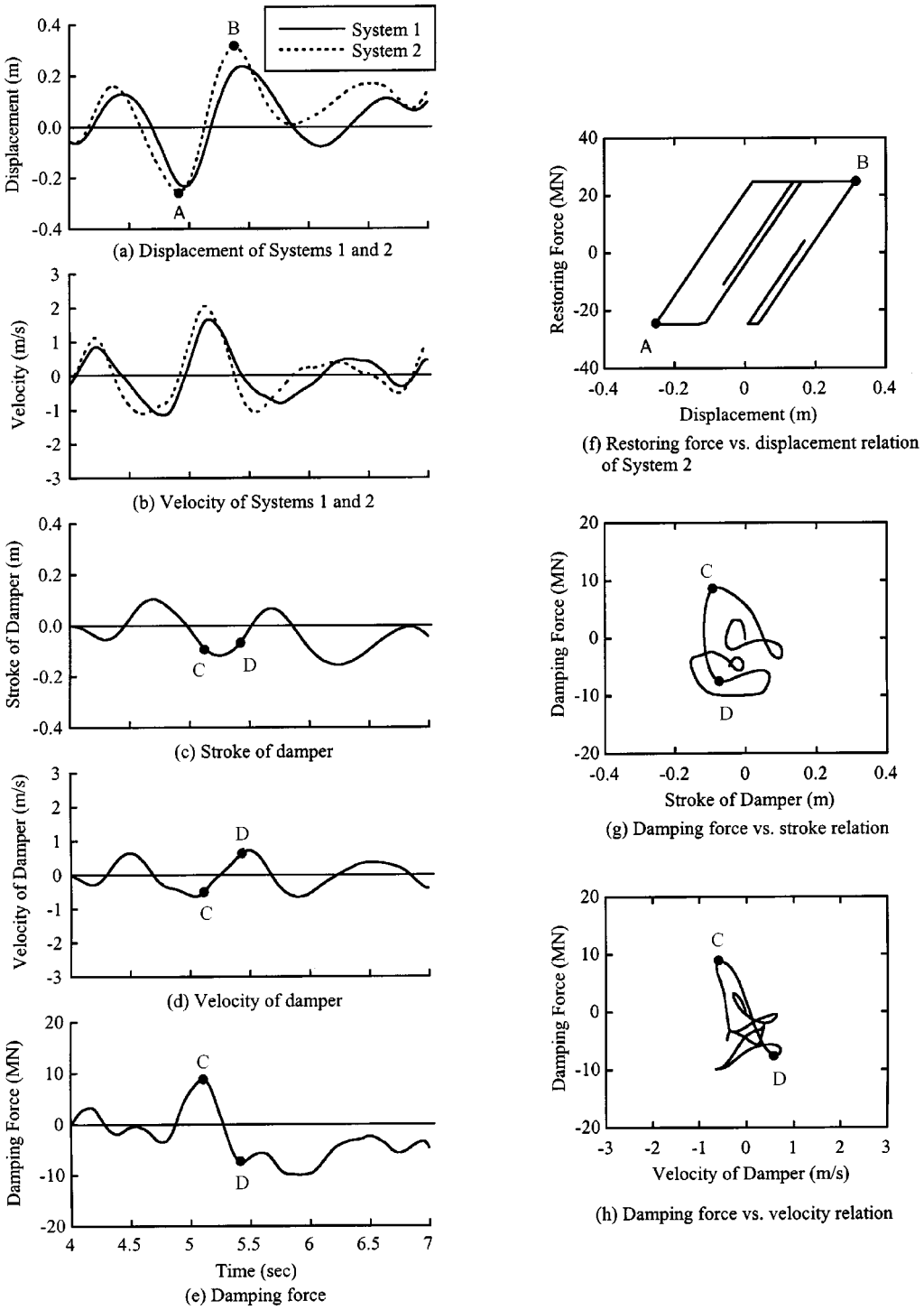

(a) Displacement of Systems 1 and 2

(b) Velocity of Systems 1 and 2

(c) Stroke of damper

(d) Velocity of damper

(e) Damping force

(f) Restoring force vs. displacement relation of System 2

(g) Damping force vs. stroke relation

(h) Damping force vs. velocity relation

Fig. 8. Explanation for the Increase of the Displacement of System 2

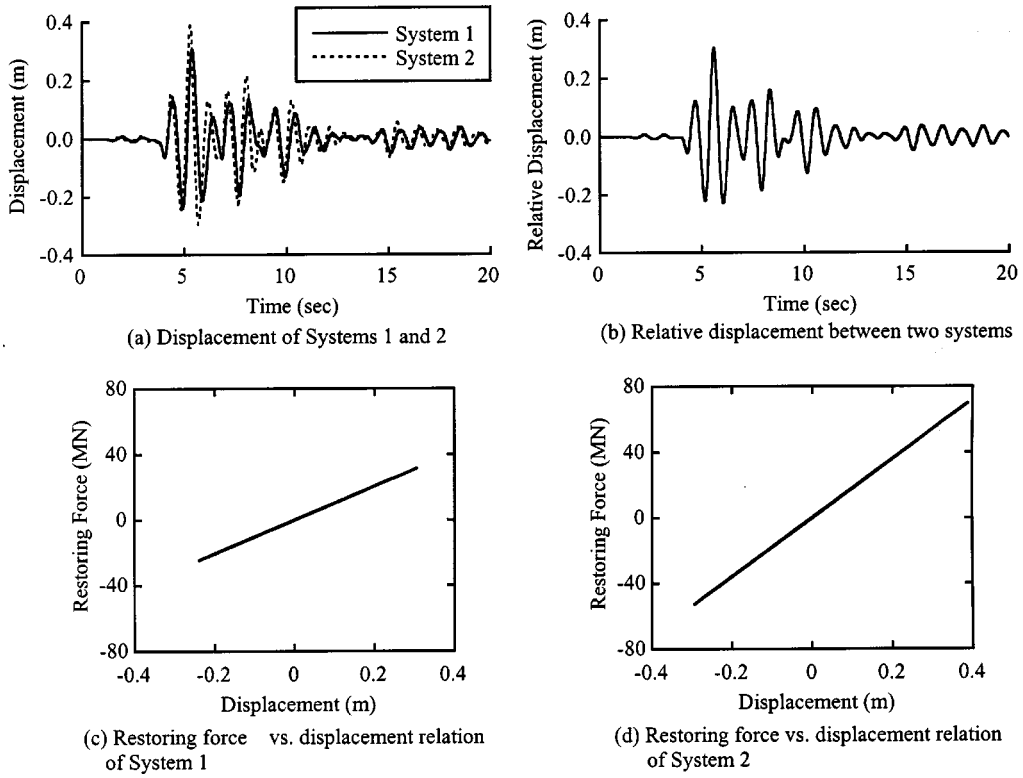

Fig. 9. Response of the Bridge with Active Control Subjected to JMA Kobe record (Linear structure)

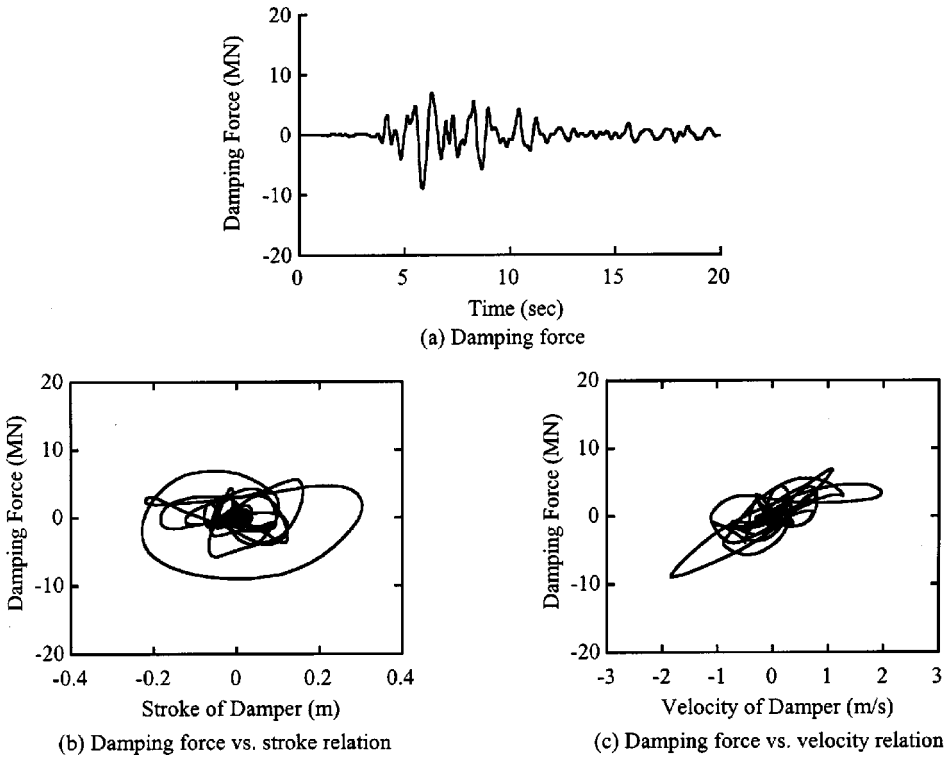

Fig. 10. Response of the Control Device with Active Control Subjected to JMA Kobe Record (Linear structure)

1.0, while that of System 2 becomes 2.27, which is close to the ductility capacity of 2.62. The displacement of System 2 was found to increase significantly when applying active control.

Fig. 7 shows the response of the active control device. Drift of damping force to negative is observed during the 6-8 s period. Note that the damping force is a function of displacement and velocity of each system. From Fig. 6 (a), a

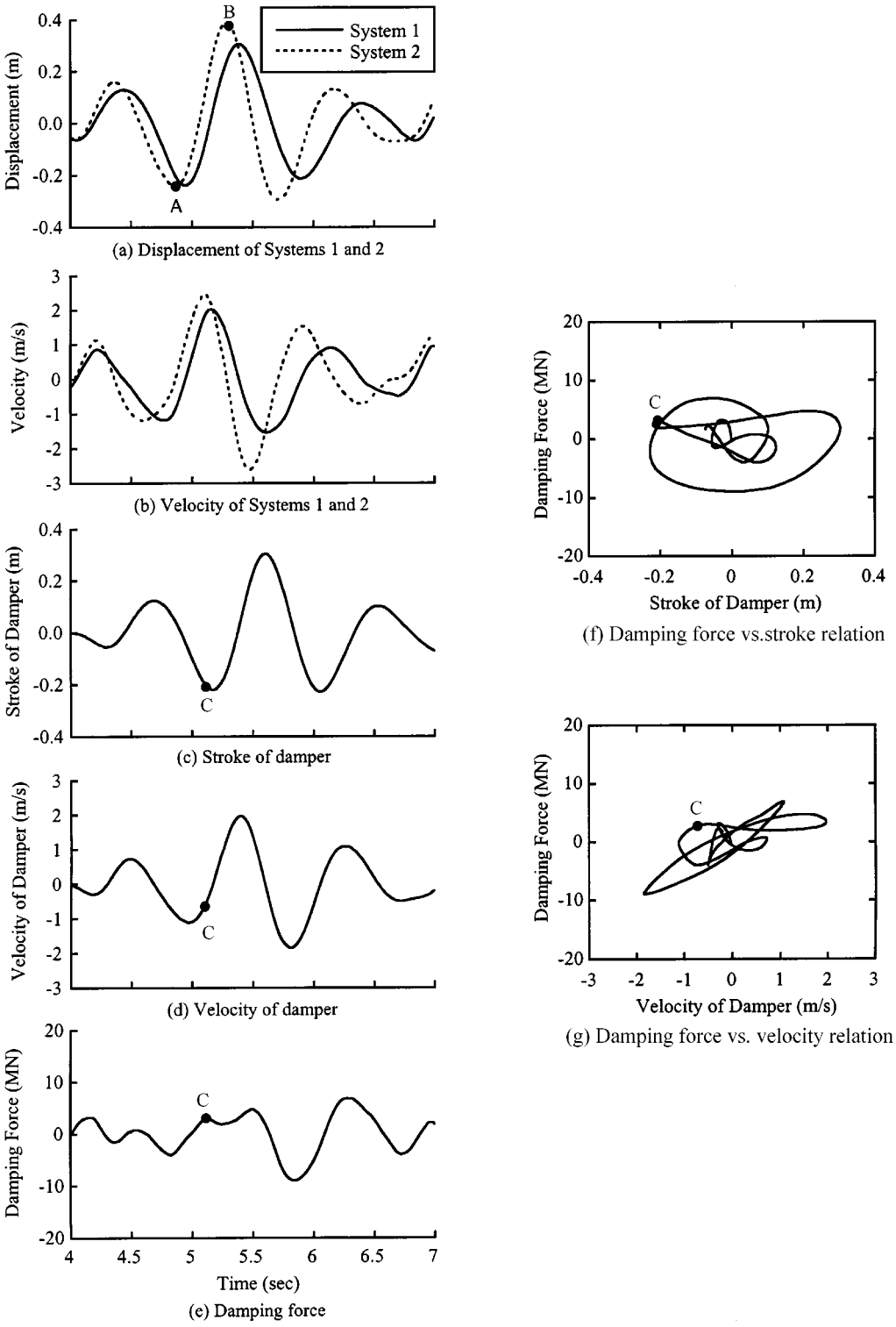

Fig. 11. Detail of Response During 4-7s

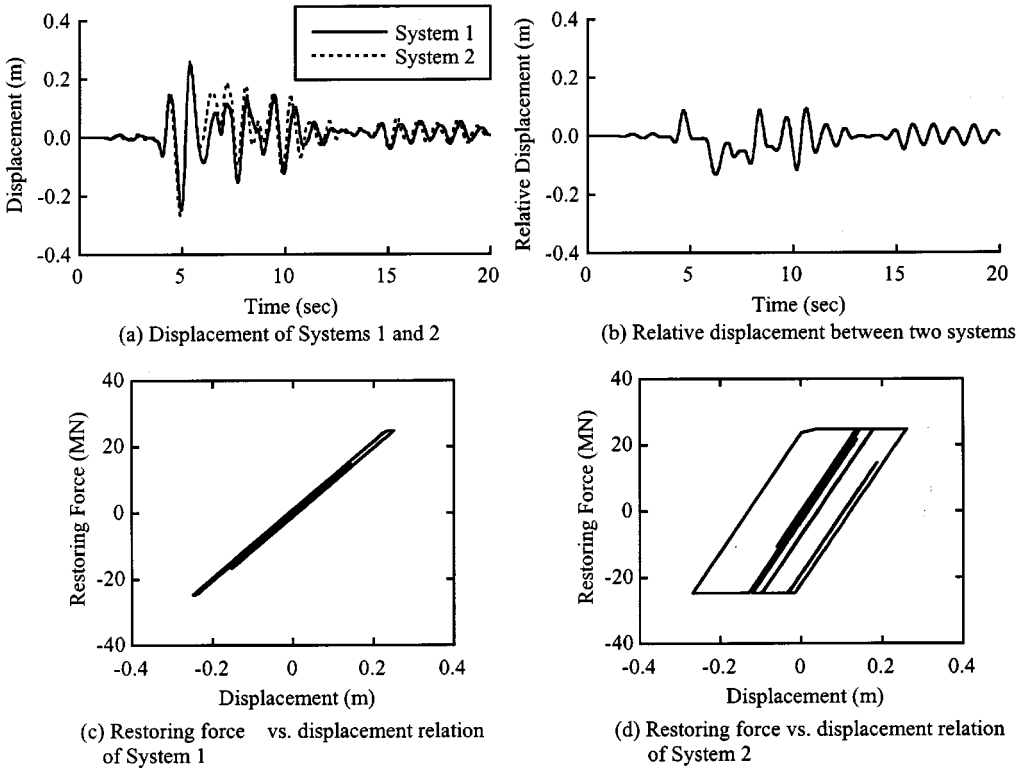

(a) Displacement of Systems 1 and 2

(b) Relative displacement between two systems

(c) Restoring force vs. displacement relation of System 1

(d) Restoring force vs. displacement relation of System 2

Fig. 12. Response of the Bridge with Semi-Active Control (JMA Kobe Record)

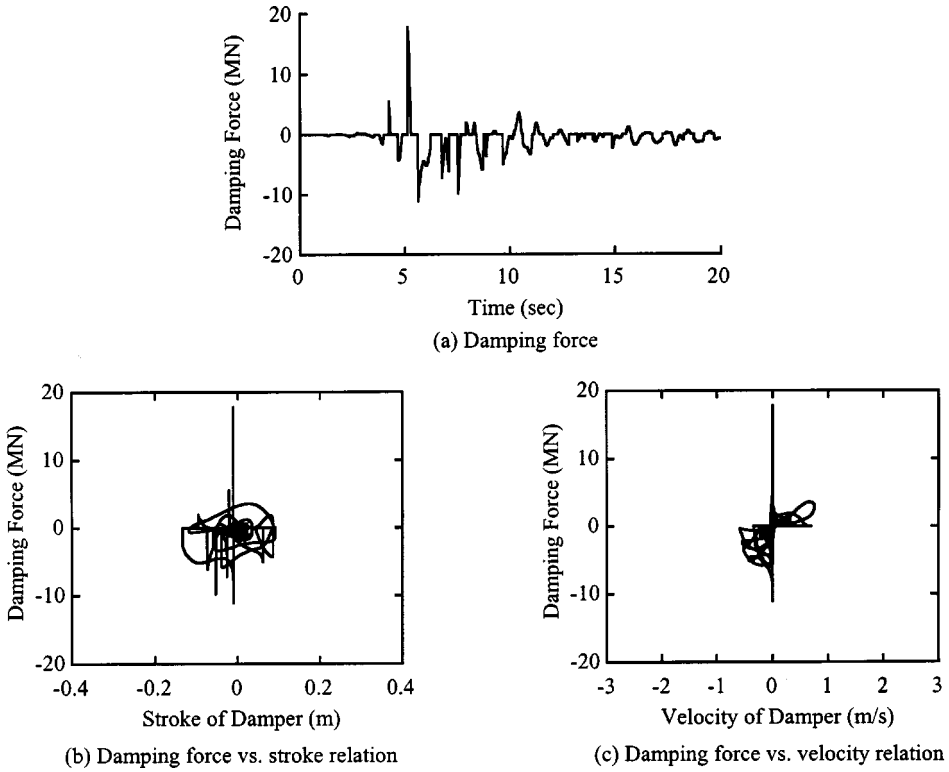

(a) Damping force

(b) Damping force vs. stroke relation

(c) Damping force vs. velocity relation

Fig. 13. Response of the Control Device with Semi-Active Control (JMA Kobe record)

drift of the displacement of System 2 is observed during the 6-8 s period. The displacement is not restored back to equilibrium position due to nonlinearity of the system. The drift of displacement results in the drift of damping force. The increase of displacement of System 2 can be explained by Fig. 8 showing the detail of response during the 4-7 s period. Focus on the movement from Point A to Point B when Systems 1 and 2 move from the maximum displacement in the negative side to the maximum displacement in the positive side. At Point C on path A-B, the damping

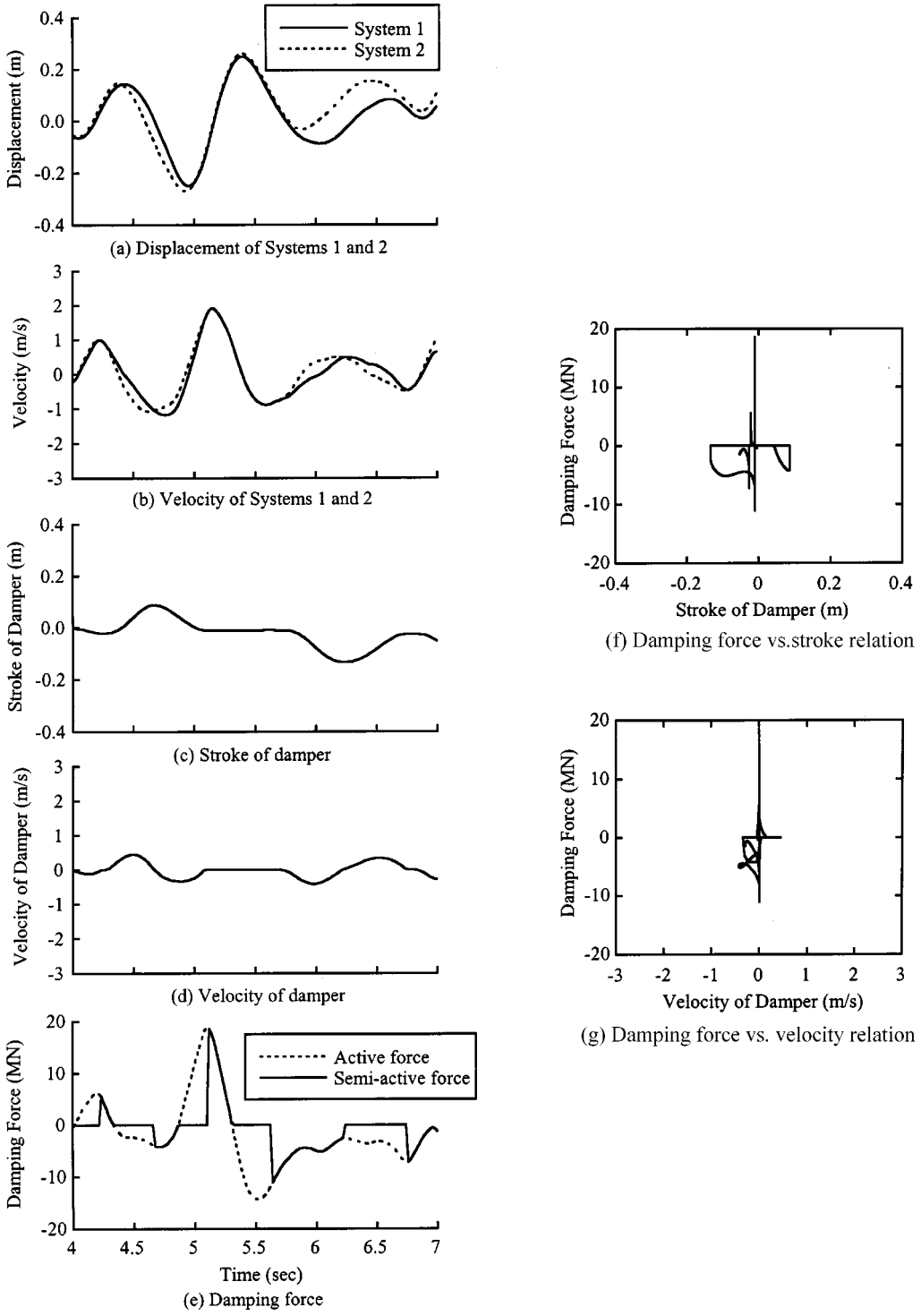

Fig. 14. Explanation for the Spikes of Damping Force

force becomes 8.8 MN while the velocity is –0.57 m/s. This condition means that the control device is pushing both systems. Consequently, the displacement of System 2 in the positive direction increases. At Point D, the sign of damping force and velocity becomes reversed, which indicates that both systems are pulled back by the device. The displacement of System 2 is restricted at Point B.

To observe how nonlinearity induced in the structure affects the control of response, the response of the linear structure is presented in Fig. 9. The maximum displacement of System 1 is 0.31 m, while that of System 2 is 0.39 m. Fig. 10 shows the response of the control device. Comparing Fig. 10 (c) to Fig. 7 (c), it is found that the damping force that has the sign opposite to the sign of velocity becomes smaller. The detail of response during 4-7 s is shown in Fig. 11. The difference of the displacement and velocity response of Systems 1 and 2 is seen to be larger than that for the nonlinear structure. This result is because when yielding of System 2 occurs, the natural period of System 2 is elongated. Thus, the response of Systems 1 and 2 tends to be more in-phase. Focus on the movement from Point A to Point B of System 2. At Point C (5.12 s) on the path A-B, the force becomes 3.04 MN, while the velocity is –0.52 m/s. This represents the condition that the control device is pushing both systems. However, the force is about 38% for the nonlinear structure. When yielding of System 2 occurs, the natural period of System 2 is elongated. The response of Systems 1 and 2 tends to get close. When the response is multiplied with the control gain matrix in Equation (9), there is the tendency that larger control force is obtained.

Fig. 12 shows the response of the bridge when the clipped optimal control is applied to control its response. The displacement of Systems 1 and 2 is 0.25 m and 0.27 m, respectively which corresponds to the response ductility factor of 1.04 and 1.95. Comparing with active control, it is seen that the response ductility factor of System 2 is significantly reduced from 2.27 to 1.95. The effectiveness of the clipped optimal control in limiting the displacement and response ductility factor of System 2 is observed. The displacement of Systems 1 and 2 are seen to be similar during the 5-5.7 s period. The relative displacement and relative velocity between the two systems are almost zero during that time. The mechanism will be described later. The response of the semi-active damper is shown in Fig. 13. There are spikes in the damping force at velocities close to zero. The maximum damping force is 17.4 MN, which is about twice that for active control. It is seen that the damping force does not exist where the damping force and velocity has the opposite signs due to the clip of damping force by the bang-bang

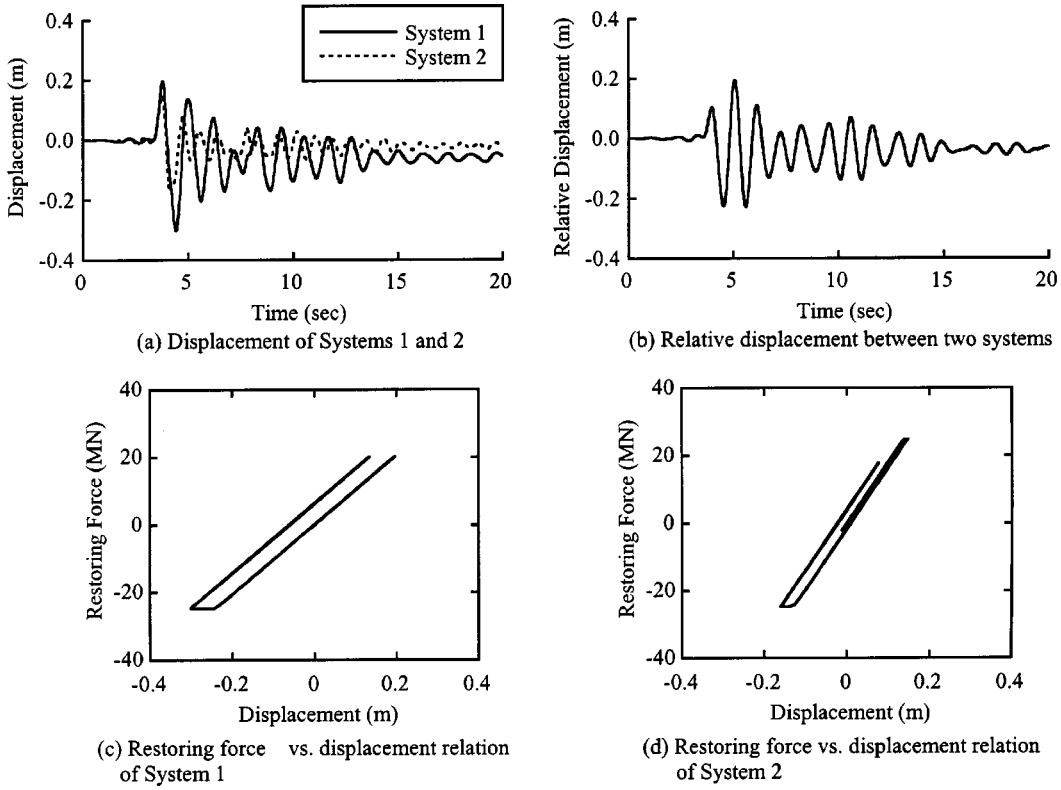

(a) Displacement of Systems 1 and 2

(b) Relative displacement between two systems

(c) Restoring force vs. displacement relation of System 1

(d) Restoring force vs. displacement relation of System 2

Fig. 15. Response of the Bridge without Control (Sylmar record)

controller. Fig. 14 illustrates response of the bridge and the damper during 4-7 s. The active force commanded by the linear optimal control and the clipped force is shown in Fig. 14 (e). When the sign of the active force and the velocity are opposite, the force is clipped to zero. When the sign of the damping force and velocity are the same, there is the sudden increase of the damping force. It can be seen that due to the sudden increase of the damping force, Systems 1 and 2 tend to be locked together. It, in turn, makes the response become more in-phase, as seen from Figs. 14 (a) and (b). The in-phase vibration tends to magnify the damping force determined by Equation (9). The phase of the damping force and the velocity of the two systems are very close. Thus, velocity of the two systems seems to be an influential factor for determining the damping force. Because the force that pushes both systems is eliminated by the bang-bang controller, the displacement of System 2 is smaller as compared to the active control.

Fig. 15 shows the response of the bridge subjected to the Sylmar record. The displacement of Systems 1 and 2 are 0.30 m and 0.16 m, respectively, corresponding to response ductility factors of 1.25 and 1.16, respectively. Both systems experience large displacements in the first few cycles, causing residual displacement of about 0.06 m and 0.03 m in Systems 1 and 2, respectively. The relative displacement between the two systems is 0.23 m. The response of the bridge with clipped optimal control is shown in Fig. 16. The response ductility factor of System 1 decreases to 1.0, while that of System 2 increases slightly to 1.23. The relative displacement between the two systems decreases to 0.11 m, which is 48% of the bridge without control. The damping force is shown in Fig. 17. The maximum damping force is 7.89 MN. A spike in the damping force is observed at 4 s, which corresponds to the time when both systems experience large response.

5. Conclusions

The clipped optimal control algorithm was extended to control the response of a nonlinear bridge model. The effectiveness of the semiactive control method for controlling a nonlinear bridge structure was investigated. Based on the analytical investigation, it may be deduced that:

1) When applying active control, the response ductility factor of a system was significantly increased by about 30%. The active control device tends to push both systems

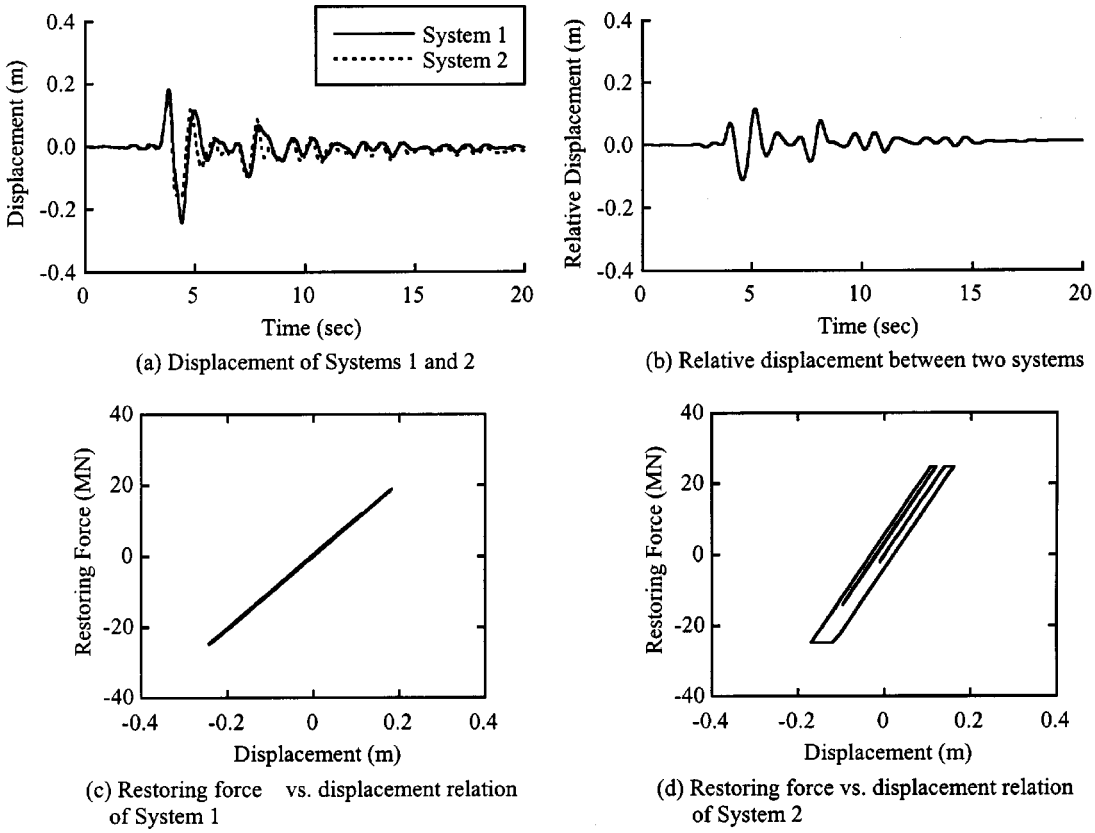

(a) Displacement of Systems 1 and 2

(b) Relative displacement between two systems

(c) Restoring force vs. displacement relation of System 1

(d) Restoring force vs. displacement relation of System 2

Fig. 16. Response of the Bridge with Semi-Active Control (Sylmar record)

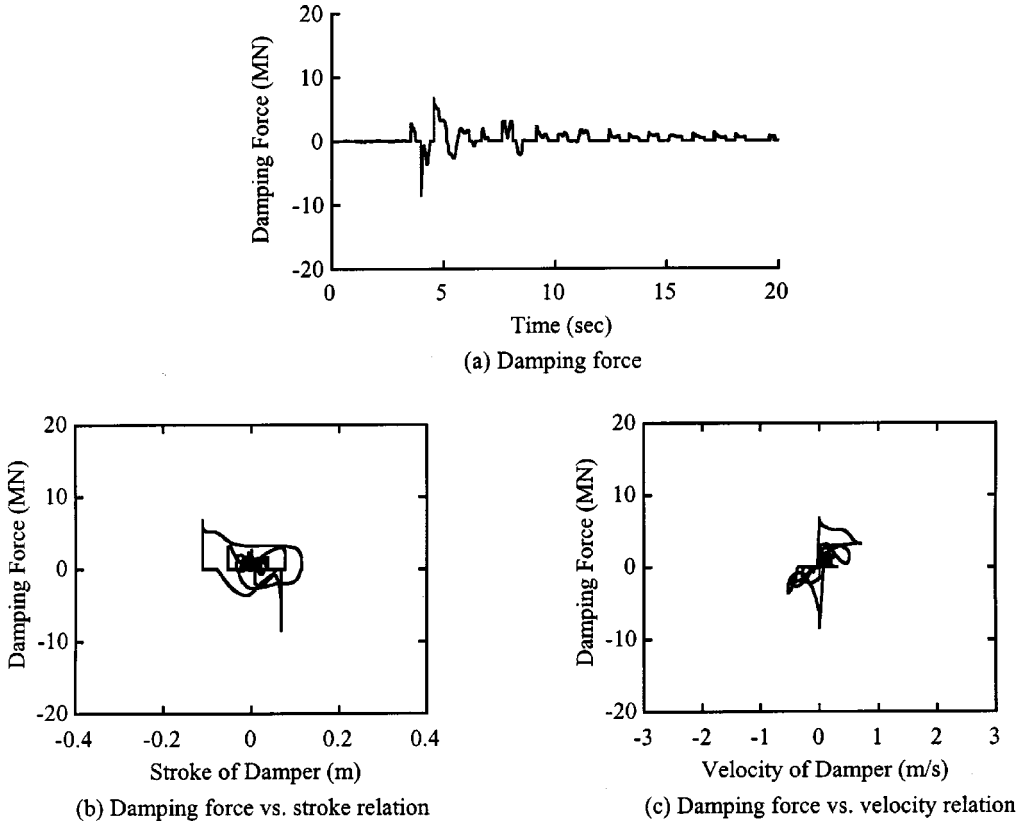

Fig. 17. Response of the Control Device with Semi-Active Control (Sylmar record)

apart due to the yielding of a structure. When a structure experiences yielding, the natural period is elongated. So, the two systems tend to vibrate in-phase. That can lead to an increase in the control force in the direction opposite to the direction of velocity and causes a significant increase in the response. Compared to active control, when semi-active control by the clipped optimal control algorithm is applied, the response ductility factor of the system can be reduced by 14%.

2) The displacement response of the two systems was intended to be controlled by providing control devices between the two decks. The displacement of one system was found to be reduced, however, the displacement of the other system was increased, resulting in an increase in the response ductility factor (e.g., in the semiactive control case, 14% reduction in the displacement of System 1, 11% increase in that of System 2, and 11% increase of the ductility factor of System 2).

3) In the clipped optimal control, a sudden increase in the force is developed in numerical simulation. In the application of the MR damper, the pulse in the damping force should be taken into account because it could induce shock in the damper. The more detailed investigation of this phenomenon should be needed.

In order to more clearly guarantee the effectiveness of the proposed method, the experiment on the coupled bridge system employing smart dampers should be performed. To do this, further studies on the system identification of the real structure, the dynamics and placements of sensors, the signal processing technique, etc. should be comprehensively accomplished and are in progress.

Acknowledgements

The authors gratefully acknowledge the support of this research by the National Research Laboratory for Aseismic Control of Structures in Korea, the 1999 Korea Research Foundation Grant, the US-Japan Cooperative Research on Urban Earthquake Disaster Mitigation, and the National Science Foundation under grant No. CMS 99-00234 (Dr. S.C. Liu, Program Director).

References

Dyke, S.J., Spencer, B.F., Jr., Sain, M.K., and Carlson, J.D. (1996). "Modeling and control of magnetorheological dampers for seismic response reduction," *Smart Materials and Structures*,

Vol. 5, 565-575.

Johnson, E.A., Ramallo, J.C., Spencer, B.F., Jr., and Sain, M.K., (1998) "Intelligent base isolation systems," *Proc. the Second World Conference on Structural Control*, Kyoto, Japan, Vol. 1, 367-376.

Spencer, B.F., Jr., and Sain, M.K. (1997). "Controlling buildings: a new frontier in feedback." *IEEE Control Systems Magazine on Emerging Technology*, Vol. 17, No. 6, 19-35.

Spencer, B.F., Jr., Dyke, S.J., Sain, M.K., and Carlson, J.D. (1997). "Phenomenological model of a magnetorheological damper." *Journal of Engineering Mechanics,* Vol. 123, No. 3, ASCE, 230-238.

Sunakoda, K., Sodeyama, H., Iwata, N., Fujitani, H., and Soda, S. (2000) "Dynamic characteristics of magneto-rheological fluid damper." *Proc. SPIE 7th Annual International Symposium on Smart Structures and Materials*, Newport Beach, USA.

Wen, Y.K. (1976). "Method for random vibration of hysteretic systems." *Journal of Engineering Mechanics Division*, Vol. 102, No. 2, ASCE, 249-263.

Yoshioka, H., Ramallo, J.C., and Spencer, B.F., Jr. (2002) "íSmartí base isolation strategies employing magnetorheological dampers," *Journal of Engineering Mechanics, ASCE*, accepted.